International Journal of Mechanical, Industrial and Aerospace Sciences
ISSN: 2517-9950
Vol:6, No:12, 2012

Stiffness Modeling of 3-PRS Mechanism

Xiaohui Han, Yuhan Wang, and Jing Shi

***Abstract*—**This paper proposed a stiffness analysis method for a 3-PRS mechanism for welding thick aluminum plate using FSW technology. In the molding process, elastic deformation of lead-screws and links are taken into account. This method is based on the virtual work principle. Through a survey of the commonly used stiffness performance indices, the minimum and maximum eigenvalues of the stiffness matrix are used to evaluate the stiffness of the 3-PRS mechanism. Furthermore, A FEA model has been constructed to verify the method. Finally, we redefined the workspace using the stiffness analysis method.

***Keywords*—**3-PRS, parallel mechanism, stiffness analysis, workspace.

I. Introduction

IN recent years, parallel mechanism has been studied and developed widely for various applications [1]. Although parallel mechanism provides small rang motion compared with series mechanism, it has some advantages that series mechanism doesn't have. For example, Parallel mechanism possesses high stiffness, high natural frequencies, vacuum compatibility and clean room compatibility. There is neither error accumulation nor backlash for the parallel structure [2].

Friction stir welding (FSW) was invented at The Welding Institute (TWI) of UK in 1991. As shown in Fig. 1, FSW uses a no consumable rotating tool with a specially designed pin and shoulder. The localized heat generated by the friction and plastic deformation between the tool and the parts to be assembled softens the material around the pin. Combination of tool rotation and translation leads to movement of material front of the pin to the back side. As a result, a sound and homogenous joint is produced in "solid state" in this welding process. However, one major disadvantage of FSW is the need of heavy-duty machinery, due to the required large forces and torques. Researchers point out that the axial force placed on the work piece by the tool is a very important process parameter, which is influenced by FSW tool's plunge depth, rotation rate, traverse rate, and pose related to parts to be jointed. So the FSW tool's pose should include the position and orientation. To the best of our knowledge, there are no mechanisms can achieve the requirements of orientation flexibility and high rigidity simultaneously. And it is the key obstacle to the development of spatial welding with FSW on serial robot solutions. One promising solution to the above problem is the use of a three-degree-of-freedom (DOF) spatial PKM of type 3-PRS.

Han Xiaohui is with the State Key Laboratory of Mechanical System and Vibration, 800 Dong Chuan Road, Shanghai 200240, China.

Yuhan Wang is with the State Key Laboratory of Mechanical System and Vibration, 800 Dong Chuan Road, Shanghai 200240, China (phone: 86-021-34206800; e-mail: yhwang@sjtu.edu.cn).

Jing Shi is with the State Key Laboratory of Mechanical System and Vibration, 800 Dong Chuan Road, Shanghai 200240, China.

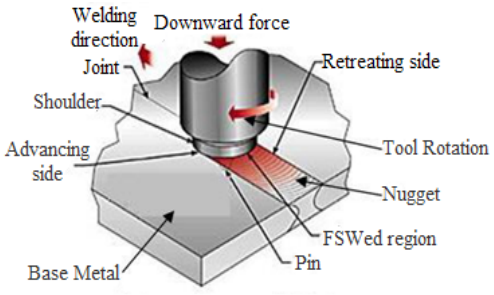

Fig. 1 Schematic description of the FSW process

The mechanical design of parallel mechanism is a process in which many criterions, such as the working space, dexterity and stiffness have to be considered [3]. So far, many researchers on parallel mechanism have been published, concerning motion analysis and singularity [4-9]. However, the evaluation of parallel mechanism's stiffness is still a tough problem. Currently, stiffness of a parallel mechanism is analyzed based on two methods: FEM modeling [10-12] and reduced analytical modeling [13-15]. FEM modeling is the most accurate computational method to investigate the stiffness of a flexure mechanism. However, this method does not establish the analytical relationship between stiffness and dimensions of the mechanism. So analytical modeling is more significant to earlier stage of design and mechanism's control. The stiffness analysis of a parallel mechanism has been studied by Arai et al. [16] and Owia et al. [17], and their studies didn't include elastic deformations. Woo-Keun Yoon, Takashi Suehiro etc. also studied the stiffness of a compact modidied delta parallel mechanism [4]. Y. Li and Q. Xu proposed a method of stiffness modeling for 3-PRS mechanism, however, which only the deformation of each actuator was considered.

In this paper, we proposed a method a stiffness modeling method of 3-PRS mechanism, in which, the deformation of lead-screws and links were taken into account. Firstly, the mechanical features of the 3-PRS mechanism are briefly addressed. Secondly, we derived the stiffness matrix for lead-screw and link and then derived the stiffness matrix for the whole 3-PRS mechanism. Thirdly, we gave the result using the method and use it to help us to determine workspace of the mechanism. Finally, we carried out stiffness analysis by using

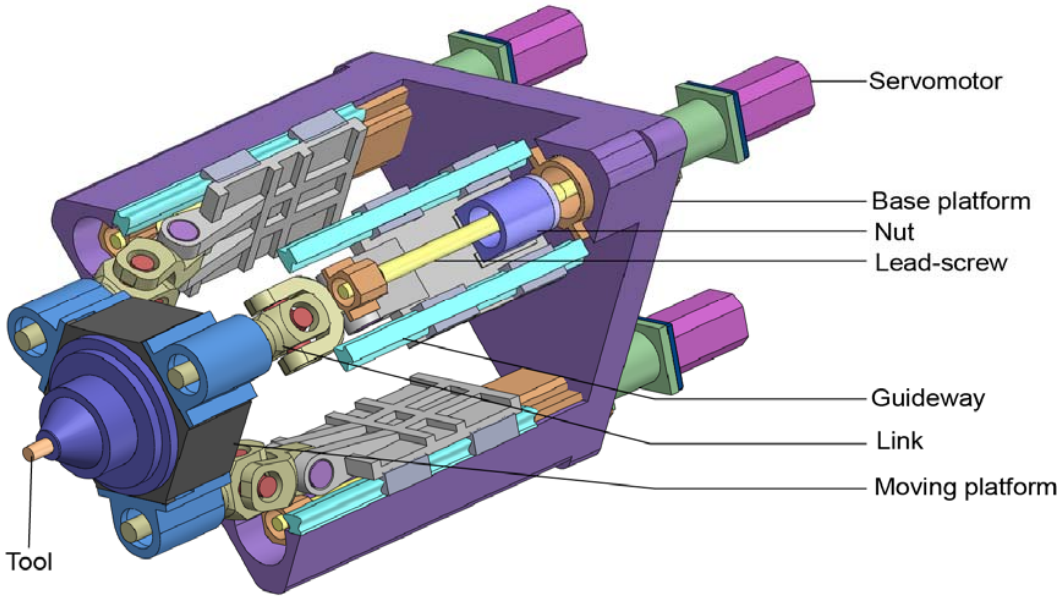

Fig. 2 3D model of 3-PRS mechanism

ANSYS and compared the deformation calculated by ANSYS to our modeling result.

II. Stiffness Modeling of 3-PRS Mechanism

A. Geometrical Description of the Mechanism

The CAD model of 3-PRS mechanism is presented in Fig. 1. The mechanism consists of a fixed base platform, a moving platform and three identical PRS limbs. In this paper, R and S represent, respectively, a revolute and a spherical joint. P denotes an active prismatic joint which are driven independently by three servomotor lead-screw assemblies. The R joints and S joints are connected by threes links severally. So the moving platform can achieve three degrees of freedom which are one translation and two rotations. The tool and spindle are mounted at the center of the moving platform.

The vectors and reference frames are described in Fig. 3. Without general, a fixed Cartesian reference coordinate frame is located at the centered point O of the fixed triangle base platform . And a body-fixed Cartesian reference coordinate frame $P-uvw$ is located at the centered point P , which is the moving triangle platform $\Delta S_1S_2S_3$, and the S_i (i=1,2,3) locates in the center of spherical joint. For the purposes of describing convenient, let the y_0-axis gets through point A_1 and $u-axis$ gets through point S_1 . Additionally, the body-fixed Cartesian reference coordinate frames of links and lead-screws are shown in Fig. 3, too.

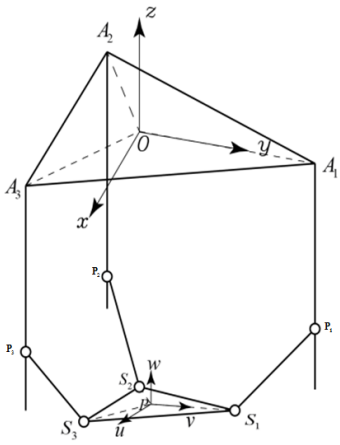

(a)

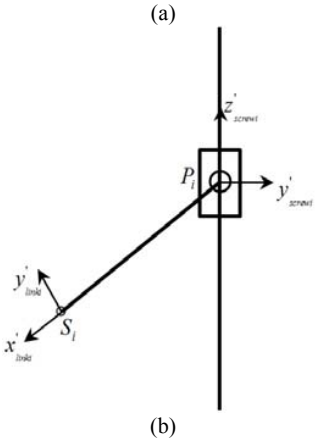

(b)

Fig. 3 The vectors and reference frames

Since the joint DOFs of each link are five, each link provide one constraint to the moving platform, so 3-PRS mechanism

possess three DOF: rotation about two perpendicular axes intersecting at the moving platform center and a horizontal plane, and a vertical translational motion [20]. In order to describe posture of 3-PRS mechanism, we use $[z \quad \alpha \quad \beta]$ to be the descriptive variable. In which, z is the z-directional component of the moving platform center referenced by coordinate system, $[\alpha \quad \beta]$ are the angle of precession and angle of nutation, respectively.

B. Stiffness Modeling of Individual Component

1. Modeling of The Link

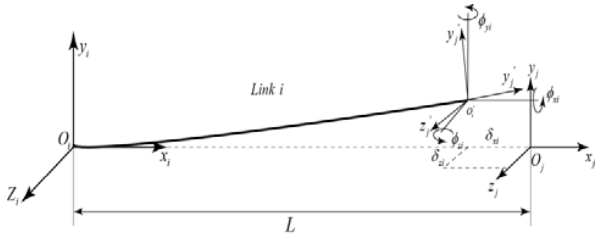

Fig. 4 Deformation at the end of link

A model describing forces and moments acting on the end of the link is shown in Fig. 4. According to mechanics of materials, elastic deformation at the end of the link can be derived as follows:

$$\begin{aligned}
\delta_{xi} &= \frac{L}{E_{link}A_{link}}F_{xi} \\
\delta_{yi} &= \frac{L^3}{3E_{link}I_y}F_{yi} + \frac{L^2}{2E_{link}I_Z}M_{Zi} \\
\delta_{zi} &= \frac{L^3}{3E_{link}I_z}F_{zi} - \frac{L^2}{2E_{link}I_y}M_{yi} \\
\phi_{xi} &= \frac{L}{G_{link}I_p}M_{xi} \\
\phi_{yi} &= -\frac{L^2}{2E_{link}I_z}F_{zi} + \frac{L}{E_{link}I_y}M_{yi} \\
\phi_{zi} &= \frac{L^2}{2E_{link}I_y}F_{yi} + \frac{L}{E_{link}I_z}M_{zi}
\end{aligned} \tag{1}$$

where E_{link} and G_{link} are the Young's modulus and shearing modulus of the link's material respectively. L is the link length. A_{link} is the cross area of the link. I_y and I_z are the geometrical moment of inertias severally. I_p is the polar moment of inertia.

For simplicity, Eq. (1) can be a matrix form as:

$$\Delta\underline{\mathbf{r}}_i = \underline{\mathbf{C}}_{ei}\underline{\mathbf{F}}_i \tag{2}$$

where,

$$\Delta\underline{\mathbf{r}}_i = [\delta_{xi} \quad \delta_{yi} \quad \delta_{zi} \quad \phi_{xi} \quad \phi_{yi} \quad \phi_{zi}]^T$$

$$\underline{\mathbf{F}}_i = [F_{xi} \quad F_{yi} \quad F_{zi} \quad M_{xi} \quad M_{xi} \quad M_{xi}]^T$$

then, $\underline{\mathbf{C}}_{ei}$, the compliance matrix of the link i is given by:

$$\underline{\mathbf{C}}_{ei} = \begin{bmatrix}
\frac{L}{E_{link}A_{link}} & 0 & 0 & 0 & 0 & 0 \\
0 & \frac{L^3}{3E_{link}I_y} & 0 & 0 & 0 & -\frac{L^2}{2E_{link}I_z} \\
0 & 0 & \frac{L^3}{3E_{link}I_z} & 0 & \frac{L^2}{2E_{link}I_y} & 0 \\
0 & 0 & 0 & \frac{L}{G_{link}I_p} & 0 & 0 \\
0 & 00 & \frac{L^2}{2E_{link}I_z} & 0 & \frac{L}{E_{link}I_y} & 0 \\
0 & -\frac{L^2}{2E_{link}I_y} & 0 & 0 & 0 & \frac{L}{E_{link}I_z}
\end{bmatrix} \tag{3}$$

and $\underline{\mathbf{C}}_e$, the elastic deformation compliance matrix for 3 links is given by:

$$\underline{\mathbf{C}}_e = \mathrm{diag}[\underline{\mathbf{C}}_{e1} \quad \underline{\mathbf{C}}_{e2} \quad \underline{\mathbf{C}}_{e3}] \tag{4}$$

So, the stiffness matrix for three links is $\underline{\mathbf{K}}_e = \underline{\mathbf{C}}_e^{-1}$.

2. Axial Stiffness of The Feed Lead-screw

When the axial stiffness of ith lead-screw is k_i, the elastic displacement in the axial direction can be obtained as below:

$$\Delta p_i = \frac{Fa_i}{k_i} \tag{5}$$

where,

Δp_i : Elastic displacement of a lead-screw system in the axial direction.

Fa_i : Applied axial force.

The axial stiffness k_{Pi} of the lead-screw system is obtained as below:

$$k_{Pi}^{-1} = k_{si}^{-1} + k_{ni}^{-1} \tag{6}$$

where,

k_{si} : Axial stiffness coefficient of the screw

k_{ni} : Axial stiffness of the nut

The axial stiffness of a screw varies depend on the method for mounting the shaft. The mounting method is present in Fig. 5.

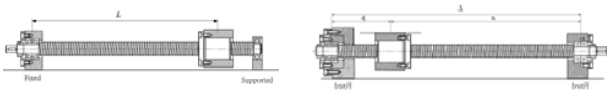

(a)Fixed-supported (b)Fixed-Fixed

Fig. 5 Mounting method of a screw

1) For fixed-supported (or -free) configuration

$$k_{si} = \frac{A_{screw} \cdot E_{screw}}{L_{screw}} \tag{7}$$

2) For fixed-fixed configuration

$$k_{si} = \frac{A_{screw} \cdot E_{screw} \cdot L_{screw}}{a_{screw} \cdot b_{screw}} \tag{8}$$

where,

A_{screw}: Screw cross-sectional area

E_{screw}: Young's modulus of the screw

L_{screw}: Distance between two mounting surfing

So, $\underline{\mathbf{K}}_P$, the stiffness matrix for 3 lead-screws is given by:

$$\underline{\mathbf{K}}_P = \mathrm{diag}[K_{p1} \quad K_{p2} \quad K_{p3}] \tag{9}$$

C. Stiffness Modeling of 3-PRS Mechanism

In this section, we derive the compliance for 3-PRS mechanism. Let $\underline{\boldsymbol{\tau}}_T = \begin{pmatrix} \underline{\mathbf{F}}^T & \underline{\mathbf{M}}^T \end{pmatrix}$ be the externally applied wrench imposed at the tool tip and $\delta \underline{\mathbf{r}}_T = \begin{pmatrix} \delta \underline{\boldsymbol{\rho}}_T & \delta \underline{\boldsymbol{\alpha}}_T \end{pmatrix}$ be the corresponding virtual deflection twist produced by $\boldsymbol{\tau}_T$. Here, $\mathbf{F}$ and $\mathbf{M}$ are the applied force and moment, $\delta\boldsymbol{\rho}$ and $\delta\boldsymbol{\alpha}$ are the linear and angular displacement at the tool tip with respect to the coordinate frame $P-uvw$, respectively. Additionally, let $\underline{\boldsymbol{\tau}}_P$ and $\underline{\boldsymbol{\tau}}_c$ be respectively the forces/torques of actuators and constraints, with respect to the body-fixed Cartesian references.

Apply the virtual work principle to the 3-PRS model:

$$\underline{\boldsymbol{\tau}}_T{}^T \delta \underline{\mathbf{r}}_T = \underline{\boldsymbol{\tau}}_p{}^T \delta \underline{\mathbf{r}}_p + \underline{\boldsymbol{\tau}}_c{}^T \delta \underline{\mathbf{r}}_c \tag{10}$$

where, $\delta \underline{\mathbf{r}}_p$ and $\delta \underline{\mathbf{r}}_c$ are the corresponding virtual deflection twist produced by $\boldsymbol{\tau}_p$ and $\boldsymbol{\tau}_c$, respectively.

According to the kinematic analysis, we can derive the Jacobian matrix $\underline{\mathbf{J}}_p$ which expresses the relationship of $\delta \underline{\mathbf{r}}_p$ and $\delta \underline{\mathbf{r}}_T$, $\underline{\mathbf{J}}_c$ which expresses the relationship of $\delta \underline{\mathbf{r}}_c$ and $\delta \underline{\mathbf{r}}_T$. So (10) can be derived as below:

$$\underline{\boldsymbol{\tau}}_T{}^T \delta \underline{\mathbf{r}}_T = \underline{\boldsymbol{\tau}}_p{}^T \underline{\mathbf{J}}_p \delta \underline{\mathbf{r}}_T + \underline{\boldsymbol{\tau}}_c{}^T \underline{\mathbf{J}}_c \delta \underline{\mathbf{r}}_c \tag{11}$$

because $\delta \mathbf{r}_T$ is arbitrary, we can derive:

$$\underline{\boldsymbol{\tau}}_T = \underline{\mathbf{J}}_p{}^T \underline{\boldsymbol{\tau}}_p + \underline{\mathbf{J}}_c{}^T \underline{\boldsymbol{\tau}}_c \tag{12}$$

take $\underline{\mathbf{K}}_e$ and $\underline{\mathbf{K}}_P$ into Eqs. (12), yields:

$$\underline{\boldsymbol{\tau}}_T = \underline{\mathbf{J}}_p{}^T \underline{\mathbf{K}}_p \delta \underline{\mathbf{r}}_p + \underline{\mathbf{J}}_c{}^T \underline{\mathbf{K}}_c \delta \underline{\mathbf{r}}_c \tag{13}$$

further, we can derive Eqs. (13) as below:

$$\underline{\boldsymbol{\tau}}_T = \underline{\mathbf{J}}_p{}^T \underline{\mathbf{K}}_p \underline{\mathbf{J}}_p \delta \underline{\mathbf{r}}_T + \underline{\mathbf{J}}_c{}^T \underline{\mathbf{K}}_c \underline{\mathbf{J}}_c \delta \underline{\mathbf{r}}_T \tag{14}$$

so (14) can be derived as:

$$\underline{\boldsymbol{\tau}}_T = \left(\underline{\mathbf{J}}_p{}^T \underline{\mathbf{K}}_p \underline{\mathbf{J}}_p + \underline{\mathbf{J}}_c{}^T \underline{\mathbf{K}}_c \underline{\mathbf{J}}_c \right) \delta \underline{\mathbf{r}}_T \tag{15}$$

finally, we write (15) as below:

$$\underline{\boldsymbol{\tau}}_T = \underline{\mathbf{K}} \delta \underline{\mathbf{r}}_T \tag{16}$$

where,

$$\underline{\mathbf{K}} = \underline{\mathbf{J}}_p{}^T \underline{\mathbf{K}}_p \underline{\mathbf{J}}_p + \underline{\mathbf{J}}_c{}^T \underline{\mathbf{K}}_c \underline{\mathbf{J}}_c \tag{17}$$

$\underline{\mathbf{K}}$ is the stiffness matrix of a general 3-PRS mechanism. We discover that the matrix is symmetric, positive. Furthermore, the stiffness matrix depends on several factors, including the size and material of the links and lead-screws, the position and posture of the moving platform.

III. Simulation Result

In this section, the geometrical and physical parameters of 3-PRS prototype are shown. And the simulation results are presented.

In order to predict the stiffness, we use the eigenvalue of the stiffness matrix as the interested stiffness factor [18,19]. The stiffness can be evaluated using the eigenvalue of the stiffness matrix which is experienced in the direction of the corresponding eigenvector [20]. It is shown that the stiffness is bounded by the minimum and maximum eigenvalues of the stiffness matrix [21]. Hence, the minimum and maximum values of stiffness and their variances appear to be the reasonable indices. The main geometrical parameters of 3-PRS are presented in Table I- Table III.

We can know from (8) that when $a_{screw} = b_{screw}$, k_{si} will be the minimum value. It means with that posture the configuration possesses the poorest stiffness. In our design, when $z = -0.4\ m$, the configuration reaches the poorest posture. And we really care is the minimum stiffness during the designing process. So analyzing the stiffness distribution in plane $z = -0.4\ m$ will be significant. The distribution for the minimum stiffness and maximum stiffness in the planes of $z = -0.4\ m$ are presented in Fig. 6.

TABLE I
THE LINK PARAMETERS

Symbol	Description	Quantity
$L(mm)$	Link length	185
$A_{link}(mm^2)$	Cross area	7200
$I_y(mm^4)$	Geometrical moment of inertias	8.64×10^6
$I_z(mm^4)$	Geometrical moment of inertias	2.16×10^6
$I_p(mm^4)$	Polar moment of inertia	1.296×10^6
$E_{link}(Pa)$	Young's modulus	2.1×10^{11}
$G_{link}(Pa)$	Radius of moving platform	8.24×10^{10}

TABLE II
THE LEAD-SCREW PARAMETERS

Symbol	Description	Quantity
$L(mm)$	Lead length	600
$A_{link}(mm^2)$	Cross area	183.5
$E_{link}(Pa)$	Young's modulus	2.31×10^{11}

TABLE III
THE OTHER MAIN PARAMETERS

Symbol	Description	Quantity
$R(mm)$	Radius of base platform	470
$r(mm)$	Radius of moving platform	315

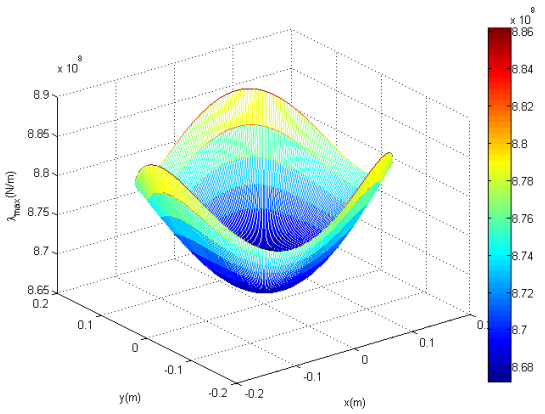

(a) Maximum stiffness map

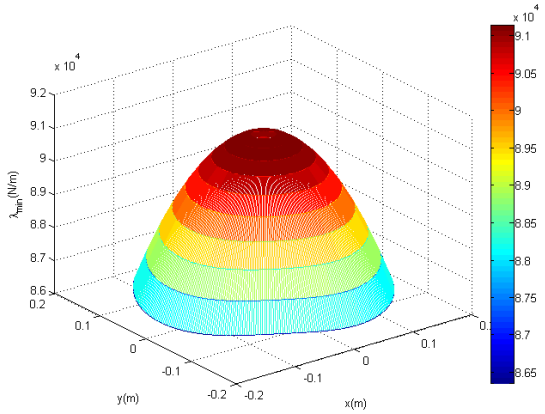

(b) Minimum stiffness map

Fig. 6 Minimum and maximum stiffness values at height of $z=-0.4m$

It can be found that the distribution of stiffness in x-y plane is 120-degree-symmetrical about the axial direction. In addition, the lowest value of minimum stiffness occurs around the boundary of the workspace, so does the highest value of the maximum stiffness. It is due to the manipulator approaches singular when it comes near the workspace boundary. It means with the nutation angle β increasing, the stiffness becomes worse and worse.

In order to verify the effectiveness of the method presented in this paper, ANSYS finite software analysis software is used to perform a stiffness analysis for the 3-PRS mechanism at the posture where $z=-0.4m$, $\alpha=0^o$ and $\beta=0^o,5^o,10^o$, respectively.

The applying force $\vec{F}=[100000N \quad 50000N \quad 50000N]$, which is referenced by body-fixed Cartesian reference coordinate $P-uvw$. The results are presented in Fig. 7.

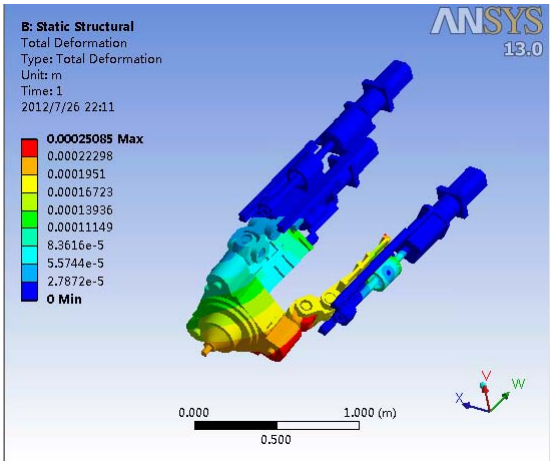

(a) $\beta=0^o$

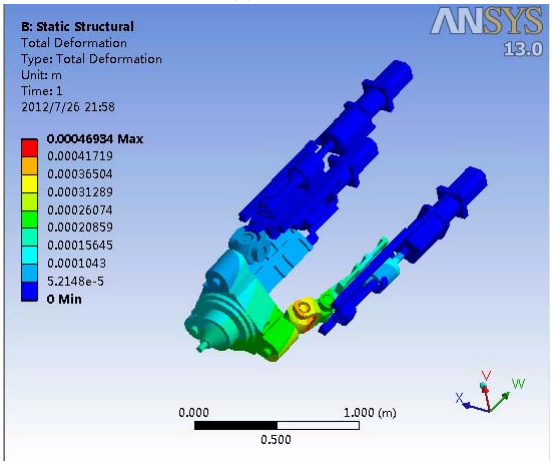

(b) $\beta=5^o$

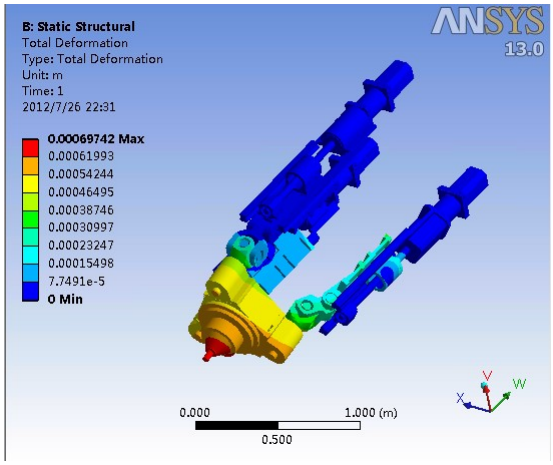

(c) $\beta = 10^o$

Fig. 7 Deformation with $\vec{F}$ imposed at tool tip

TABLE IV
SIMULATION RESULTS COMPARISON

	$\beta = 0^o$	$\beta = 5^o$	$\beta = 10^o$
Analytical deformation	0.25mm	0.47mm	0.69mm
FEA deformation	0.21mm	0.42mm	0.61mm

Table IV summarize the result of analytical modeling and FEA modeling. It can be seen that the results of the analytical modeling match well with the results of FEA modeling. Besides, we can find the analytical results are smaller than the FEA results. The reason is that in the analytical modeling, the deformations of joints were not taken in account. Furthermore, we can find the deformation becomes larger with the nutation angle β increasing, which coincide with our analysis of Fig. 6.

Because the mechanism possesses a bad stiffness property around the boundary of the reachable workspace, it is necessarily to restrict the manipulator to work near the boundary when 3-PRS mechanism is used in heavy-duty situation.

Furthermore, the reachable workspace of a 3-PRS mechanism is usually used as workspace which is defined according singularity analysis and dexterity analysis. This definition method is only built on the kinematic foundation without considering the load property. In fact, when the mechanism hasn't reached the singularity point, the stiffness is poor enough so that the machine isn't qualified for the heavy-duty machining near the singularity point. So it's necessary to redefine the workspace by taking singularity analysis, dexterity analysis and stiffness analysis into account simultaneously.

In order to redefine the workspace, a numerical searching method can be adopted to evaluate the minimum stiffness indices throughout the reachable space. According to the 3-PRS tasks and performances, a stiffness lower limit is determined. Then we can divide the reachable workspace into small pieces and check piece-by-piece to confirm whether the current piece belongs to the workspace. The size of the samples is dependent on the required accuracy. Once the search completed, the redefined workspace is determined. We can find the redefined workspace is the subspace of the reachable workspace.

Fig. 8 present the refined workspace using the method mentioned in this paper. The redefined workspace is 120-degree-symmetrical about the axial direction, too. Moreover, the range of tool tip movement in plane $z = -0.4m$ is smaller. The phenomenon corresponds to our analysis in the beginning of part III.

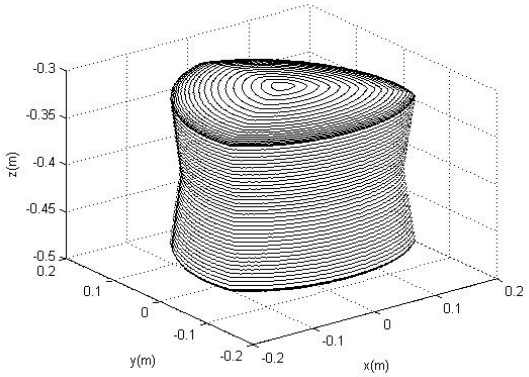

Fig. 8 The redefined workspace

IV. CONCLUSION

In this paper, we proposed a stiffness analysis method for a 3-PRS mechanism, which takes into account elastic deformation of lead-screws and links. This method is based on the virtual work principle. Though a survey of the commonly used stiffness performance indices, the minimum and maximum eigenvalues of the stiffness matrix are used to evaluate the stiffness of the 3-PRS mechanism. The stiffness model can be used as a tool to predict the stiffness in the workspace. Moreover, the stiffness estimation can help to optimize the design of the 3-PRS mechanism. Furthermore, A FEA model has been constructed to verify the method.

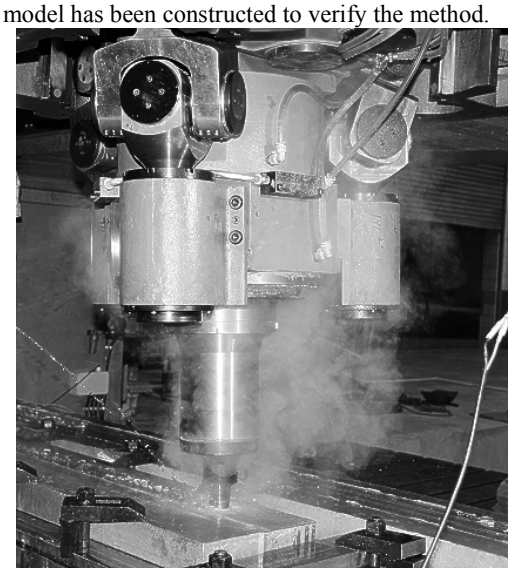

Fig. 9 Prototype of the proposed tool head for friction stir welding

REFERENCES

[1] J.-P. Merlet, Parallel Robots, Kluwer Academic Publishers, London,2000
[2] Huy-Hoang Pham, I-Ming Chen, Stiffness modeling of flexure parallel mechanism, Precision Engineering 29 (2005) 467-478.
[3] Clement Gosselin, Stiffness Mapping for Parallel Manipulators, IEEE Transactions On Robotics And Automation, Vol. 6, No.3, June 1990.
[4] Woo-Keun Yoon, Takashi Suehiro, Yuichi Tsumaki and Masaru Uchiyama, Stiffness Analysis and Design of a Compact Modified Delta Parallel Mechanism, Robotica (2004) volume 22, pp, 463-475.
[5] R. E. Stamper, L. W. Tsai and G. C. Walsh, "Optimization of a Three DOF Translational Platform for Well-Conditioned Workspace," Proc. of the 1997 IEEE Int. Conf. on Robotics and Automation (1997) pp. 3250–3255.
[6] L. Baron and J. Angeles, "The Direct Kinematics of Parallel Manipulators Under Joint-Sensor Redundancy," IEEE Transactions on Robotics and Automation 16(1), 12–19 (2000).
[7] M. J. Liu, C. X. Li and C. N. Li, Dynamics Analysis of the Gough-Stewart Platform Manipulator, IEEE Transactions on Robotics and Automation 16(1), 94–99 (2000).
[8] J. E. McInroy and J. C. Hamann, Design and Control of Flexure Jointed Hexapods, IEEE Transactions on Robotics and Automation 16(4), 372–381 (2000).
[9] X. J. Liu, J.Wang, F. Gao and L. P.Wang, "Mechanism design of a simplified 6-DOF 6-RUS parallel manipulator," Robotica 20(1), 81–91 (2002).
[10] Woronko A, Huang J, Altintas Y. Piezoelectric tool actuator for precision machining on conventional CNC turning centers. Prec Eng 2003;27:335–45.
[11] Zhang S, Fasse E. A finite-element-based method to determine the spatial stiffness properties of a notch hinge. ASME J Mech Des 2001;123:141–7.
[12] Xu G, Qu L. Some analytical problems of high performance flexure hinge and micro-motion stage design. In: Proceedings of IEEE International Conference on Industrial Technology. 1996.p. 771–5.
[13] Lobontiu N. Compliant mechanisms: design of flexure hinges. 2nd ed. CRC Press; 2003.
[14] Henein S, Bottinelli S, Clavel R. Parallel spring stages with flexures of micrometric cross-sections. In: Proceedings of the SPIE on Microrobotics and Micro-system Fabrication, vol. 3202. 2001. p. 209–20.
[15] Alici G, Shirinzadeh B. Kinematics and stiffness analyses of a flexure-jointed planar micromanipulation system for a decoupled compliant motion. In: Proceedings of IEEE International Conference on Intelligent Robots and Systems. 2003. p. 3282–7.
[16] T. Arai, Analysis and Synthesis of a Parallel Link Manipulator Based on Its Statics, J. Robotics Society of Japan 10(4), 526–533 (1992) (in Japanese).
[17] T. Oiwa and M. Hirano, Six Degree-of-Freedom Fine Motion Mechanism using Parallel Mechanism – Link Layout Design-, J. the Japan Society for Precision Engineering 65(10), 1425–1429 (1999) (in Japanese).
[18] C. Gosselin, Stiffness mapping for parallel manipulators, IEEE Trans. Robot. Automat. 6 (3) (1990) 377–382.
[19] N. Simaan, M. Shoham, Stiffness synthesis of a variable geometry six-degrees-of-freedom double planar parallel robot, Int. J. Robot. Res. 22 (9) (2003) 757–775.
[20] Yangmin Li, Qingsong Xu, Stiffness analysis for a 3-PUU parallel kinematic machine, Mechanism and machine Theory 43 (2008) 186-200.
[21] B.S. El-Khasawneh, P.M. Ferreira, Computation of stiffness and stiffness bounds for parallel link manipulators, Int. J. Mach. Tools Manuf. 39 (2) (1999) 321–342.